NONLINEAR WAVE INTERACTION WITH SUBMERGED AND SURFACE-PIERCING POROUS STRUCTURES

Okey Nwogu[1] and Zeki Demirbilek[2]

A coupled Boussinesq-boundary integral method is developed to simulate nonlinear water wave interaction with structures consisting of multiple layers with different physical and hydraulic characteristics. The flow field in the water region is modeled with a modified set of Boussinesq-type equations, with additional terms to account for the flow of water into/out of the porous region. The equations of motion for the porous regions include an empirical Forchheimer-type term for laminar and turbulent frictional losses, and an inertial term for acceleration effects. A boundary integral formulation based on Green's third identity is used to close the problem for the porous region. The coupled equations for the evolution of the free surface and boundary values of the tangential velocities are integrated in time using an iterative Crank-Nicolson scheme. At each time step, the Boussinesq problem is solved for the water region to determine the pressure at porous interface. The boundary integral problem for the porous region is then solved to determine the normal velocities along porous interface. The model is used to investigate wave interaction with a vertical surface-piercing porous structure and wave transmission over submerged breakwaters. Comparisons between the numerical model predictions and laboratory data show generally good agreement for both the wave field inside the structure and the reflection/transmission coefficients.

1. INTRODUCTION

Porous structures such as rubblemound breakwaters typically consist of multiple dissipative layers with different physical and hydraulic characteristics. A better understanding of the dissipation, reflection and transmission characteristics of porous structures is required to accurately predict wave conditions in navigation channels and harbors, sediment dynamics behind submerged breakwaters, and erosion and sedimentation processes near coastal inlets.

Early theoretical studies of wave-porous bed interaction were concerned with the attenuation of surface waves propagating over permeable horizontal seabeds (e.g. Putnam, 1949; Reid and Kajiura, 1957). Linear wave theory was used to describe the overlying wave field while Darcy's law was used to describe the flow inside the porous layer. Darcy's law is valid for flows with low Reynolds number. As the flow velocity or particle size increases, Darcy's linear relationship between the discharge velocity and pressure gradient breaks down and the quadratic drag law proposed by Forchheimer (1901) becomes more applicable. Sollitt and Cross (1972) presented a modified set of equations

[1] Dept. of Naval Architecture and Marine Eng., University of Michigan, Ann Arbor, MI, 48109-2145, U.S.A.
[2] Coastal and Hydraulics Lab., U.S. Army Engineer R & D Center, Vicksburg, MS,

for fluid motion within a porous medium that included both a Forchheimer-type drag term and inertial effects. An eigenfunction expansion method was used to solve the linearized form of the equations for waves normally incident on vertical surface-piercing porous structures.

In many applications, it is important to investigate wave propagation over non-horizontal seabeds or wave interaction with non-rectangular breakwaters. The porous medium could also consist of multiple layers with different porosities and dissipative properties. Several investigators (e.g. Sulisz 1985; Mallayachari and Sundar 1994) have used linear boundary integral methods to simulate wave interaction with multi-layer porous structures. Linear models, however, cannot accurately describe the nonlinear wave steepening and breaking processes that occur on the slopes of submerged and surface-piercing trapezoidal structures. These complicated processes can be better addressed by numerically solving either the full Navier-Stokes equations (e.g. Liu *et al*. 1999) or asymptotic theories for weakly nonlinear/weakly dispersive waves.

Flaten and Rygg (1991) developed an asymptotic Boussinesq-type theory for shallow water wave propagation over a permeable bed. Darcy's law was used to model the flow inside the porous layer. Cruz *et al*. (1997) developed a two-layer weakly nonlinear Boussinesq model that included both fluid acceleration effects and quadratic drag losses inside the porous layer. The dispersive and damping properties of the equations were also improved by introducing additional dispersive terms to the momentum equations using the approach of Madsen and Sorensen (1992). Hsiao *et al*. (2002) extended the two-layer approach to large amplitude waves by using a fully nonlinear set of Boussinesq equations for the water region. While the two-layer Boussinesq approach is suitable for modeling wave propagation over permeable seabeds, it is not ideal for studying wave interaction with multi-layer porous structures of arbitrary cross-section. The equations assume that the thicknesses of the porous layers are much smaller than the incident wavelength and the interfacial/seabed slopes are mildly varying. For structures that are a fraction of a wavelength, the spatial discretization schemes used for the open water region are also too coarse to resolve details of the flow field inside the porous structure.

In this paper, a numerical model is presented for simulating nonlinear wave interaction with multi-layer porous structures of arbitrary shape. The coupled model consists of a set of fully nonlinear Boussinesq equations for the water region and boundary integral equations for each of the porous layers. This approach does not make any assumption as to the profile of the flow field inside the porous medium. The numerical model is initially calibrated with data from laboratory experiments on wave interaction with a vertical porous breakwater (Requejo *et al*. 2002). The numerical model is then used to investigate wave transmission over submerged breakwaters and compared with the laboratory data of Seabrook and Hall (1998).

2. THEORETICAL BACKGROUND

Governing Equations for Water Region

Consider the interaction of weakly dispersive surface waves with a multi-layered surface-piercing breakwater as shown in Figure 1. A fully nonlinear set of Boussinesq equations is used to describe the fluid motion in the water region. The evolution of the free surface $\eta(\boldsymbol{x},t)$ is governed by the depth-integrated mass conservation equation:

$$\eta_t + \nabla \cdot \boldsymbol{Q} = q_n^{(p)} \tag{1}$$

where $\nabla = (\partial/\partial x, \partial/\partial y)$, $\eta(\boldsymbol{x},t)$ is the water surface elevation, $q_n^{(p)}$ represents the normal flow through the water-porous layer interface and $\boldsymbol{Q}(\boldsymbol{x},t)$ is the volume flux density given by:

$$\boldsymbol{Q} = \int_{-h}^{\eta} \boldsymbol{u}^{(w)}\, dz \tag{2}$$

$\boldsymbol{u}^{(w)}$ is the horizontal fluid velocity in the water region and $h(\boldsymbol{x})$ is the water depth.

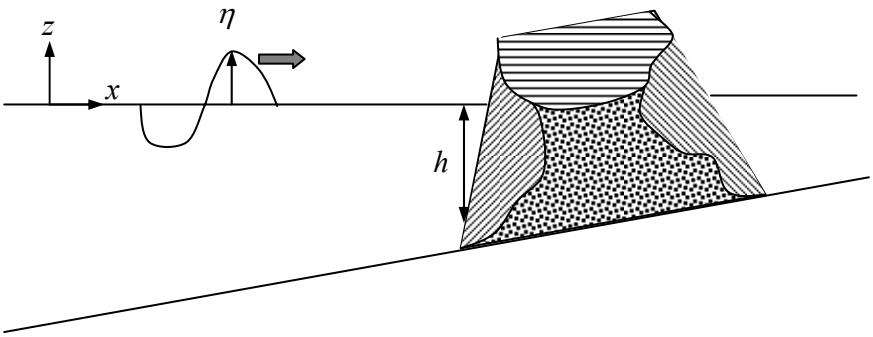

Figure 1. Definition Sketch.

The momentum equation is derived by evaluating the Euler equations at the free surface to obtain:

$$\boldsymbol{u}_t^{(w)}\Big|_\eta + w_t^{(w)}\Big|_\eta \nabla\eta + g\nabla\eta + \left(\boldsymbol{u}_\eta^{(w)} \cdot \nabla\right)\boldsymbol{u}_\eta^{(w)} + w_\eta^{(w)} \nabla w_\eta^{(w)} = 0 \tag{3}$$

where $w^{(w)}$ is the vertical velocity. The system of equations (1) to (3) requires knowledge of the vertical profile of the flow field in order to evaluate the horizontal and vertical velocities at the free surface and the volume flux density. For shallow water waves, the vertical profile of the flow field is obtained by

expanding the velocity potential, Φ, as a Taylor series about an arbitrary elevation, z_α, in the water column (Nwogu 1993):

$$\Phi^{(w)}(\boldsymbol{x},z,t) \quad = \quad \phi_\alpha + (z - z_\alpha)\left.\frac{\partial \phi^{(w)}}{\partial z}\right|_{z=-h} + \frac{1}{2}\left[(z_\alpha + h)^2 - (z + h)^2\right]\nabla^2\phi_\alpha \quad (4)$$

where $\phi_\alpha = \Phi^{(w)}(\boldsymbol{x},z,t)$. The vertical velocity at the bottom of the water region depends on the inflow/outflow from the porous region and is obtained by enforcing the continuity of normal velocity at the water-porous layer interface:

$$\left.\frac{\partial \phi^{(w)}}{\partial z}\right|_{z=-h} + \boldsymbol{u}^{(w)}\cdot\nabla h \quad = \quad \left.\frac{\partial \phi^{(p)}}{\partial n}\right|_{z=-h}\sqrt{1+\nabla h\cdot\nabla h} \quad = \quad q_n^{(p)} \qquad (5)$$

By substituting Eq. (5) into Eq. (4) and differentiating, we obtain the vertical distributions of the horizontal and vertical velocities as:

$$\begin{aligned}\boldsymbol{u}^{(w)}(\boldsymbol{x},z,t) \quad = \quad \nabla\Phi^{(w)} \quad &= \quad \boldsymbol{u}_\alpha + (z_\alpha - z)\left[\nabla(\boldsymbol{u}_\alpha\cdot\nabla h) + (\nabla\cdot\boldsymbol{u}_\alpha)\nabla h - \nabla q_n^{(p)}\right] \\ &+ \quad \frac{1}{2}\left[(z_\alpha + h)^2 - (z+h)^2\right]\nabla(\nabla\cdot\boldsymbol{u}_\alpha)\end{aligned} \qquad (6)$$

$$w^{(w)}(\boldsymbol{x},z,t) \quad = \quad \frac{\partial\Phi^{(w)}}{\partial z} \quad = \quad q_n^{(p)} - \left[\boldsymbol{u}_\alpha\cdot\nabla h + (z+h)\nabla\cdot\boldsymbol{u}_\alpha\right] \qquad (7)$$

where the velocity variable $\boldsymbol{u}_\alpha = \boldsymbol{u}(\boldsymbol{x},z_\alpha,t)$ is the horizontal velocity at $z = z_\alpha$. The volume flux density required to evaluate the mass conservation equation is obtained by substituting Eq. (6) into Eq. (2) and integrating to yield:

$$\begin{aligned}\boldsymbol{Q} \quad = \quad (h+\eta)\Bigg\{\boldsymbol{u}_\alpha + &\left[\frac{(z_\alpha+h)^2}{2} - \frac{(h+\eta)^2}{6}\right]\nabla(\nabla\cdot\boldsymbol{u}_\alpha) + \\ &\left[(z_\alpha+h) - \frac{(h+\eta)}{2}\right]\left[\nabla(\boldsymbol{u}_\alpha\cdot\nabla h) + (\nabla\cdot\boldsymbol{u}_\alpha)\nabla h - \nabla q_n^{(p)}\right]\Bigg\}\end{aligned} \qquad (8)$$

The momentum equation can be written in terms of the velocity variable $\boldsymbol{u}_\alpha$ by substituting the expressions for $\boldsymbol{u}^{(w)}$ and $w^{(w)}$ (Eqs. 6 and 7) into Eq. 3 to obtain:

$$\begin{aligned}&\boldsymbol{u}_{\alpha,t} + g\nabla\eta + \left(\boldsymbol{u}_\eta^{(w)}\cdot\nabla\right)\boldsymbol{u}_\eta^{(w)} + w_\eta^{(w)}\nabla w_\eta^{(w)} + (z_\alpha - \eta)\left[\nabla\left(\boldsymbol{u}_{\alpha,t}\cdot\nabla h\right) + (\nabla\cdot\boldsymbol{u}_{\alpha,t})\nabla h - q_{n,t}^{(p)}\right] \\ &+ \frac{1}{2}\left[(z_\alpha+h)^2 - (h+\eta)^2\right]\nabla\left(\nabla\cdot\boldsymbol{u}_{\alpha,t}\right) - \left[\left(\boldsymbol{u}_{\alpha,t}\cdot\nabla h\right) + (h+\eta)\nabla\cdot\boldsymbol{u}_{\alpha,t} - q_{n,t}^{(p)}\right]\nabla\eta \\ &+ \frac{1}{h+\eta}f_w\boldsymbol{u}_b^{(w)}\left|\boldsymbol{u}_b^{(w)}\right| + \frac{1}{h+\eta}\nabla\left(\nu(h+\eta)\nabla\cdot\boldsymbol{u}_\alpha\right) \quad = \quad 0\end{aligned} \qquad (9)$$

where ν and f_w are the eddy viscosity and bottom friction coefficient respectively intended to account for wave energy dissipation due to wave breaking and bottom friction. The wave breaking model is based on the eddy viscosity model of Nwogu (1996).

Equations (1), (8) and (9) represent a modified set of fully nonlinear Boussinesq equations for the water region. Compared to the fully nonlinear equations of Nwogu (1996), Eqs. (1) and (9) contain additional terms involving $q_n^{(p)}$ to account for flow into and out of the porous structure. The normal flow through the water-porous layer interface will be determined by solving a boundary value problem for the porous region.

Governing Equations for Porous Region

The asymptotic Taylor series expansion used to describe the flow field in the water region could also be applied to shallow porous layers (e.g. Hsiao *et al*., 2002). However, this approach is cumbersome to apply to structures that consist of multiple porous layers of arbitrary cross-sections. Since the flow inside the porous layer satisfies the Laplace equation, Green's third identity may be applied over any closed boundary S to relate the values of the potential inside the bounded region with the boundary values of the velocity potential $\Phi^{(p)}(\boldsymbol{\xi})$ and its normal derivative $\partial\Phi^{(p)}(\boldsymbol{\xi})/\partial n$. For field points $\boldsymbol{x}$ that lie along the boundary, the velocity potential is given by:

$$\Phi^{(p)}(\boldsymbol{x}) = \frac{1}{\pi}\oint_S \left[G(\boldsymbol{x};\boldsymbol{\xi})\frac{\partial\Phi^{(p)}}{\partial n}(\boldsymbol{\xi}) - \Phi^{(p)}(\boldsymbol{\xi})\frac{\partial G}{\partial n}(\boldsymbol{x};\boldsymbol{\xi}) \right] dS \qquad (10)$$

where $G = -\ln|\boldsymbol{x}-\boldsymbol{\xi}|$ is the Greens function and $\boldsymbol{\xi}$ represents the source point on the boundary S over which the integration is performed. The integral equation is evaluated numerically by dividing the porous layer boundaries into a finite number of segments with the values of $\Phi^{(p)}$ and $\partial\Phi^{(p)}/\partial n$ assumed to be constant over each segment and defined at the midpoints of the segments. The integral equation for each porous region can thus be rewritten as a matrix equation in terms of discrete values of $\Phi^{(p)}$ and $\partial\Phi^{(p)}/\partial n$:

$$\sum_{j=1}^{N}\left\{ \left[A_{ij} + \delta_{ij}\right]\Phi_j^{(p)} + B_{ij}\frac{\partial\Phi_j^{(p)}}{\partial n} \right\} = 0 \qquad (11)$$

where N is the number of segments on the boundary and the matrix coefficients A_{ij}, B_{ij} correspond to the integral of the Green's function or its normal derivative over the individual segments. When $i \neq j$, the integrals are approximated by assuming the Green's function (or normal derivative) to be constant over each segment and evaluated at the midpoint of the segment. When $i = j$, the integrals become singular and are evaluated analytically.

Each porous layer may have up to four different types of boundary conditions corresponding to: 1) matching boundary with water region, 2) free

surface, 3) matching boundary with another porous layer, and 4) impermeable boundary.

Along matching boundaries with the water region, we enforce the continuity of pressure and normal velocities. The solution of the problem for the water region provides pressure boundary conditions for the porous layer while the solution for the porous layer provides normal velocity boundary conditions for the water region. Following Sollitt and Cross (1972), we assume that the flow in the porous region is governed by a Forchheimer-type resistance term plus an inertial term to account for fluid acceleration around solid particles. The continuity of pressure boundary condition is obtained by evaluating the modified Euler equations for the porous region along the interface $z = z_i$. This can be expressed in terms of the tangential velocity along the interface $q_s^{(p)} = \nabla\Phi^{(p)}$ as:

$$\begin{aligned} & c_m \boldsymbol{q}_{s,t}^{(p)} + g\nabla z_i + \frac{c_m}{\lambda}\left(\boldsymbol{u}_i^{(p)} \cdot \nabla\right)\boldsymbol{u}_i^{(p)} + \frac{c_m}{\lambda} w_i^{(p)} \nabla w_i^{(p)} \\ & + f_l \lambda \boldsymbol{q}_s^{(p)} + f_t \lambda \boldsymbol{q}_s^{(p)} \sqrt{\boldsymbol{u}_i^{(p)} \cdot \boldsymbol{u}_i^{(p)} + w_i^{(p)2}} = -\frac{1}{\rho}\lambda \nabla p_i^{(w)} \end{aligned} \tag{12}$$

where c_m is an inertial coefficient, which can be written in terms of the added mass coefficient, c_a, using $c_m = 1 + (1-\lambda)\, c_a$, λ is the effective porosity of the medium, $(\boldsymbol{u}_i^{(p)}, w_i^{(p)})$ are the discharge velocities on the porous layer side of the interface, and f_l and f_t are empirical laminar and turbulent friction factors. The friction factors can be related to the permeability of the medium (Sollitt and Cross, 1972) or the characteristic stone size, d, and porosity by (e.g. Van Gent 1995):

$$\begin{aligned} f_l &= a_0 \frac{(1-\lambda)^2}{\lambda^3}\frac{\nu}{d^2} \\ f_t &= b_0\left(1 + \frac{7.5}{K_C}\right)\frac{(1-\lambda)}{\lambda^3}\frac{1}{d} \end{aligned} \tag{13}$$

a_0, and b_0 are empirical constants, and $K_C = \pi H/(\lambda d)$ is the Keulegan-Carpenter number with H the characteristic wave height. The empirical coefficients depend on the particle shape, surface roughness and Reynolds number of the flow.

The pressure boundary condition (Eq. 12) is also applied along phreatic surface boundaries in the porous region with $z_i = \eta$ and $p_i = 0$. The location of the phreatic surface is obtained by solving the kinematic free surface boundary condition:

$$\eta_t = \frac{1}{\lambda}\frac{\partial\Phi^{(p)}}{\partial n}\sqrt{1 + \nabla\eta \cdot \nabla\eta} \tag{14}$$

The normal velocities $\partial\Phi^{(p)}/\partial n$ are obtained as part of the solution of the boundary integral equation.

Along matching boundaries between porous layers, we enforce the continuity of $\Phi^{(p)}$ and $\partial\Phi^{(p)}/\partial n$ while the zero normal flow boundary condition ($\partial\Phi^{(p)}/\partial n = 0$) is enforced along impermeable boundaries.

Numerical Solution

The governing mass and momentum equations for the evolution of the free/phreatic surfaces and velocity variables are integrated in time using a modified Crank-Nicolson scheme. At each time step, we initially solve the Boussinesq problem for water region to determine the pressure forcing along all porous interfacial boundaries. The porous-region momentum equation is then integrated to determine the velocity potential along the interface while the kinematic boundary condition is integrated to update the location of the phreatic surface. The boundary integral problem for the porous region is then solved to determine normal velocities along the interfacial boundaries. Finally, the Boussinesq problem is re-solved with updated values of the normal velocity along porous interface. This procedure is repeated at each time step until convergence.

3. NUMERICAL RESULTS

Wave Interaction with a Vertical Surface-Piercing Breakwater

The performance of the numerical model was initially evaluated with data from the laboratory experiments of Requejo *et al*. (2002), who investigated the interaction of periodic waves with a crib-style rectangular breakwater. The experiments were conducted in a 12-m long and 0.56-m wide wave flume using two structure widths (B = 0.56m, 1.12m), two characteristic stone sizes (d = 0.0105m, 0.0378m), three wave periods (T = 1.2s, 1.7s, 2.7s), and five wave heights (H = 0.02m to 0.09m). Five wave probes were used to measure the wave field in front of the structure and two or three wave probes were used to measure inside the structure. The experimental layout is shown in Fig. 2.

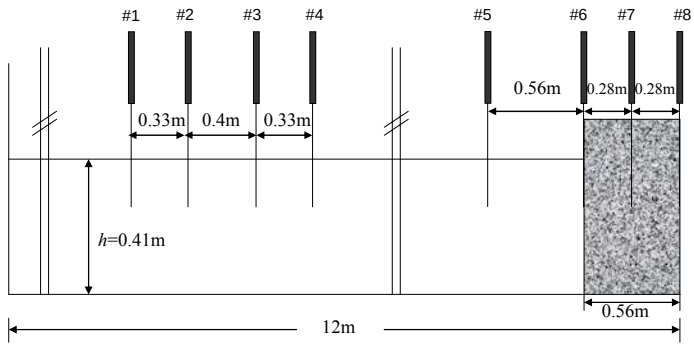

Figure 2. Layout of laboratory experiments of Requejo *et al*. (2002).

Table 1. Summary of Best-Fit Empirical Constants for *H*=0.034m, *T*=1.7s.

Structure	*B(m)*	*d*(m)	a_o	b_o
#1	1.12	0.0105	100	1.5
#2	0.56	0.0105	100	1.5
#3	1.12	0.0378	100	0.6
#4	0.56	0.0378	100	0.6

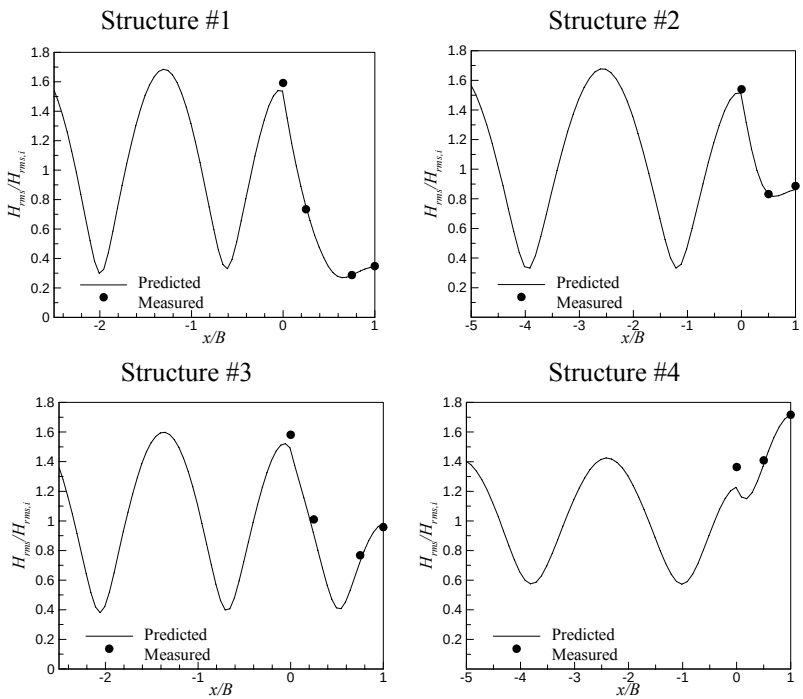

Figure 3. Comparison of measured and predicted wave heights for *H*=0.034m, *T*=1.7s.

We investigated the sensitivity of the numerical model predictions of the wave heights inside the porous structure to the values of the empirical constants a_o, b_o. Numerical simulations were carried out for one of the test conditions (H = 0.034m, T = 1.7s) for different combinations of a_o and b_o, with a_o varying from 0 to 300, and b_o from 0 to 3. These range of values were selected to cover the optimal values a_o = 100 and b_o = 1.1 recommended by Requejo *et al*. (2002). The value c_a = 0.4 was used for added mass coefficient as suggested by Van Gent (1995). The values of a_o and b_o that yielded the least square error between

the measured and predicted wave heights inside the structure are summarized in Table 1. The empirical constant b_o associated with turbulent losses was smaller for Structures #3 and #4 that have the larger stone size.

The numerically simulated wave height distributions with the best-fit coefficients are compared to the measured wave heights in Figure 3. Although the reflection coefficients were similar for some of the test conditions, the different structures have fairly different wave height variations inside the structure. Excellent agreement is observed between the measured and predicted wave heights inside the structure for Structures #1, #2, and #3.

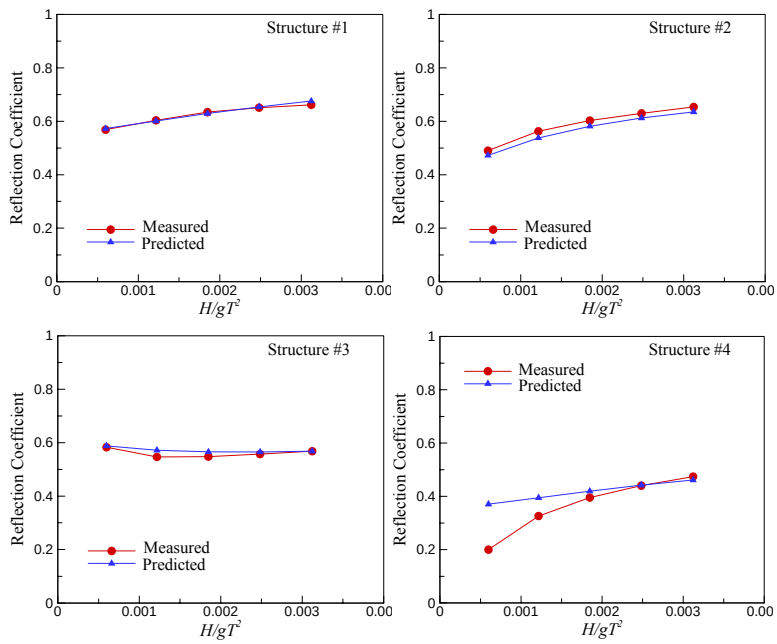

Figure 4. Measured and predicted reflection coefficients (*T* = 1.7s).

The best-fit empirical constants for Structures #3 and #4 (a_o = 100, b_o = 0.6) were used in numerical simulations for other wave conditions and structure configurations to investigate the potential relative error in using a universal set of constants to estimate the reflection properties of porous structures. The measured and computed reflection coefficients are shown in Figure 4 for T =1.7s, and Figure 5 for T = 1.2s. Excellent agreement is observed between the predicted and measured reflection coefficients for Structures #1, #2 and #3 for T = 1.7s. The numerical model also reproduces the observed trends in the variation of reflection coefficient with wave steepness. For the T = 1.2s test conditions, the numerical model predicts larger values of the reflection coefficient (5-25%) but generally reproduces the correct trends in the variation of reflection coefficient with wave steepness.

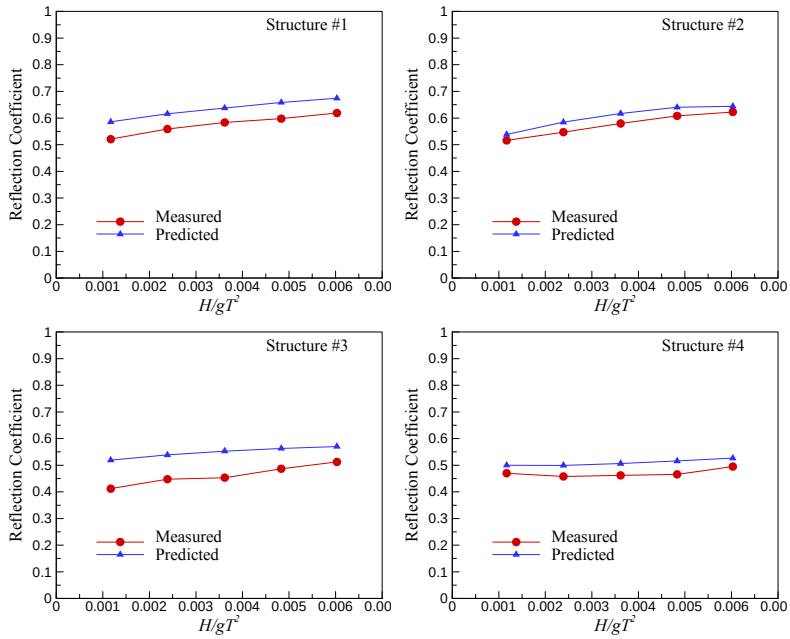

Figure 5. Measured and predicted reflection coefficients (*T* = 1.2s).

Wave Propagation over a Submerged Breakwater

Seabrook and Hall (1998) carried out an extensive series of tests to investigate wave transmission over submerged rubblemound breakwaters. The tests were conducted in a 47-m long and 1-m wide wave flume at Queens University, Canada. The layout for the experiments is shown in Figure 6. The breakwater cross-section had a crest height of h_s = 0.25m and 1V:3H side slopes. The breakwater consisted of a relatively coarse inner core layer with d_{50} = 0.017m and two layers of primary armor with d = 0.059m. Over 800 irregular wave tests were performed with 13 breakwater geometries, 5 water levels, 3 spectral peak periods, and 4 significant wave heights.

Since the transmission coefficient for submerged breakwaters depends on parameters such as the relative submergence depth and relative crest width, we carried out two sets of numerical simulations. The first set of simulations were conducted for a constant crest width B = 0.6 m and varying submergence depths d_s = 0.05, 0.1, 0.15 and 0.2m. For the second set of simulations, we varied the crest width B = 0.6, 1.5, 2.5 and 3.5m and used a submergence depth of 0.05m. The numerical simulations were performed for an incident sea state characterized by a JONSWAP spectrum with H_{mo} = 0.1 m, T_p = 1.5 s and γ = 3.3. A porosity of 0.5 and empirical constants a_o = 100, b_o = 0.6, and c_a = 0.4 were used for the model simulations.

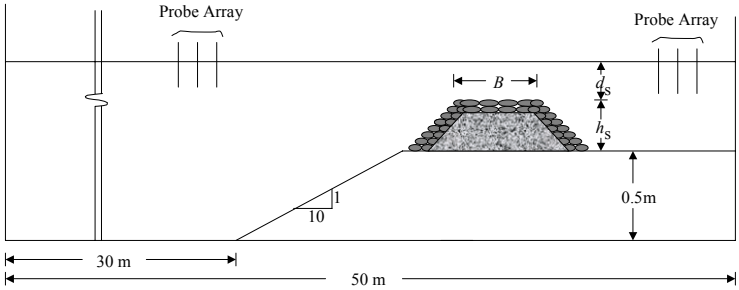

Figure 6. Layout for the Seabrook and Hall (1998) experiments.

Figure 7 shows a comparison of the variation of the measured and predicted transmission coefficients with relative submergence depth, d_s. For non-breaking waves with $d_s/H_{mo} = 2$, the transmitted wave height is about 80% of the incident wave height. As d_s decreases, the transmitted height decreases to about 40% of the incident wave height. Wave breaking over the breakwater also plays an important role in the wave energy dissipation process. Figure 9 shows a comparison of the wave transmission coefficient as a function of the breakwater crest width for a submergence depth of 0.05m. The results show a decrease in transmission coefficient with increasing crest width due to both wave breaking and energy dissipation inside the porous structure.

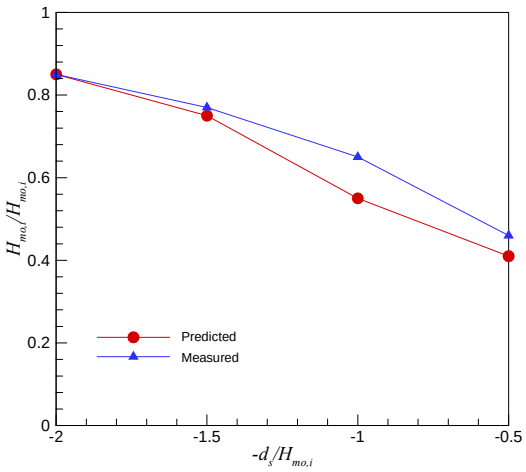

Figure 7. Variation of transmission coefficient with relative submergence depth.

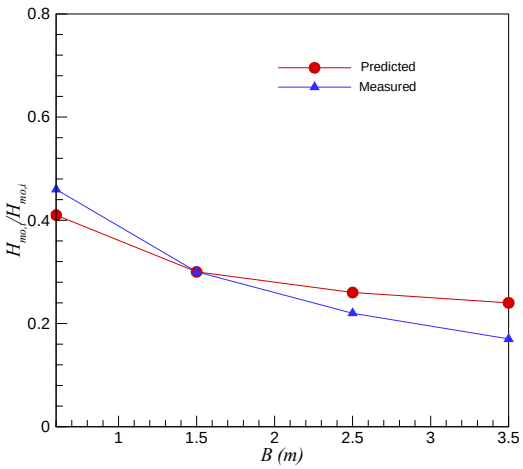

Figure 8. Variation of transmission coefficient with structure crest width.

CONCLUDING REMARKS

A coupled Boussinesq-boundary integral model has been developed to simulate nonlinear wave interaction with surface-piercing and submerged porous structures. The model solves vertically integrated Boussinesq-type equations for the water region and evolution equations for the phreatic surface and boundary values of the tangential velocities in the porous region. A boundary integral method is used to close the problem for porous region and determine the relationship between the normal and tangential velocities along the boundaries. Since the energy dissipation within porous structures is governed by empirical laminar and turbulent frictional factors, the applicability of the model formulation and determination of the friction factors have been investigated by comparing numerical model predictions of wave reflection and transmission coefficients through porous breakwaters with data from two laboratory experiments. Overall, the model performed reasonably well and was able to reproduce the observed variation of reflection coefficient with wave steepness with one set of empirical constants. Good agreement was also observed for the wave field inside the structure, provided the empirical coefficients are suitably chosen.

ACKNOWLEDGMENTS

This work was supported by the Coastal Inlets Research Program of the U.S. Army Engineer Research and Development Center. Permission to publish this paper was granted by the Chief of Engineers, U.S. Army Corps of Engineers. The authors would also like to thank C. Vidal and S.R. Seabrook for providing their laboratory data.

REFERENCES

Cruz, E. C., Isobe, M. and A. Watanabe. 1997. Boussinesq equations for wave transformation on porous beds. *Coastal Eng.*, **30**, 125–156.

Flaten G., and O.B. Rygg. 1991. Dispersive shallow water waves over a porous seabed, *Coastal Eng*., **15**, 347-369.

Forchheimer, P., 1901. Wasserbewegung durch boden. *Z.* Ver. Deutsch. Ing., **45**, 1782-1788.

Hsiao, S.-C., Liu, P.L.-F., and Y. Chen. 2002. Nonlinear water waves propagating over a permeable bed, *Proc. R. Soc. Lond. A*, **458**, 1291–1322.

Liu, P. L.-F., Lin, P., Chang, K.-A. and T. Sakakiyama. 1999. Numerical modeling of wave interaction with porous structures, *J. Waterw. Port Coastal Ocean Eng*., **125**, 322–330.

Madsen, P.A., and O.R. Sørensen. 1992. A new form of the Boussinesq equations with improved linear dispersion characteristics. Part 2. A slowly varying bathymetry, *Coastal Eng*., **18**, 183–204.

Mallayachari, V., and V. Sundar. 1994. Reflection characteristics of permeable seawalls, *Coastal Eng.*, **23**, 135-150.

Nwogu, O., 1993. Alternative form of Boussinesq equations for nearshore wave propagation, *J. Waterw. Port Coastal Ocean Eng.*, **119**, 618-638.

Nwogu, O.G., 1996. Numerical Prediction of breaking waves and currents with a Boussinesq model. *Proc. 25th Int. Conf. on Coastal Eng*., ASCE, 4807-4820.

Putnam, J.A., 1949. Loss of wave energy due to percolation in a permeable sea bottom. *Trans. Am. Geophys. Union*, **30**, 349-356.

Reid, R.O. and K. Kajiura. 1957. On the damping of gravity waves over a permeable sea bed, *Trans. Am. Geophys. Union*, **38**, 662-666.

Requejo, S., Vidal, C., and I.J. Losada. 2002. Modelling of wave loads and hydraulic performance of vertical permeable structures. *Coastal Eng*., **46**, 249-276.

Seabrook, S.R., Hall, K.R., 1998. Wave transmission at submerged rubblemound structures, *Proc. 26th Int. Conf. on Coastal Eng.*, ASCE, Copenhagen, Denmark, pp. 2000-2013.

Sollitt, C.K., Cross, R.H., 1972. Wave transmission through permeable breakwaters. *Proc. 15th Int. Conf. on Coastal Eng*., ASCE, 1827-1846.

Sulisz, W., 1985. Wave reflection and transmission at permeable breakwaters of arbitrary cross-section. *Coastal Eng*., 9, 371-386.

Van Gent, M.R.A., 1995. Wave interaction with permeable coastal structures. Ph.D. Thesis, Delft University of Technology, Delft, The Netherlands.